Shape-Selective Synthesis, Magnetic Properties, and Catalytic Activity of Single Crystalline β-MnO2 Nanoparticles

ARTICLE *in* THE JOURNAL OF PHYSICAL CHEMISTRY C · NOVEMBER 2007

Impact Factor: 4.77 · DOI: 10.1021/jp074803l · Source: OAI

Shape-Selective Synthesis, Magnetic Properties, and Catalytic Activity of Single Crystalline β-MnO_2 Nanoparticles

Subhra Jana, Soumen Basu, Surojit Pande, Sujit Kumar Ghosh, and Tarasankar Pal*

Department of Chemistry, Indian Institute of Technology, Kharagpur 721 302, India

Received: June 20, 2007; In Final Form: July 20, 2007

The shape-controlled synthesis of exclusively single crystalline β-MnO_2, nanospheres on one hand and nanorods on the other, has been achieved through air oxidation of $MnCl_2$ in variable SDBS micellar templates under alkaline condition at room temperature. Raman measurement and TEM unequivocally confirm the changes in the structural aspects of the particles from sphere to rod. Field-dependent magnetization measurement indicates superparamagnetic nature of MnO_2 rods and spheres having a blocking temperature of 4 and 40 K, respectively. These observations together with other physical parameters explicitly confirm the changes in the structural aspects of the particles with the changes in surfactant concentration. Thus, nanorods of high aspect ratio ($\sim$25) were obtained exclusively leaving aside the embryonic spherical particles (5 ± 2 nm) at lower surfactant concentration. This Article also focuses for the first time on the change in magnetic properties and cyclic voltammograms when we enroute nanospheres to nanorods. The catalytic activity of spherical and rod shaped particles has also been demonstrated.

1. Introduction

Nanostructures and nanomaterials have been the subject of intensive research throughout the world due to their potential applications in electronics, photonics, and catalysis.[1,2] One-dimensional (1-D) magnetic nanostructured materials have the ability to make great contributions in the way of microelectronic and biomedical technology. Their size alone brings forth a rich combination of optical, electronic, and magnetic properties because of their anisotropic morphologies, distinguished from their bulk counterparts and even from spherical nanoparticles of the same composition.[3,4] Such applications include magnetic memory storage, magnetic transport of biochemical complexes, and magnetic resonance imaging (MRI) enhancement.[5,6] The key to prepare a 1-D nanostructure can be focused on the way in which atoms or other building blocks are rationally assembled into structure with nanometer size but much larger lengths.

Over the past few years, manganese dioxide materials have received extensive attention due to their outstanding structural flexibility combined with novel chemical and physical properties and now are widely used as catalysts,[7] soft magnetic materials, ion-sieves, and especially as electrode materials in Li/MnO_2 batteries.[8] It is well known that manganese dioxide is a non-stoichiometric compound and can exist in different structural forms, α-, β-, γ-, and δ-types, when the basic structural unit, [MnO_6] octahedron, is linked in different ways; for example, β-MnO_2 is composed of single chains of the [MnO_6] octahedron.[8] It is generally recognized that their performance is highly dependent on their morphologies as well as crystallographic forms. Therefore, the development of the solution-based and morphologically controllable synthesis of MnO_2 nanoparticles is urgently important to answer the demand for exploring the potentials of manganese dioxide.[9,10]

Up to now, numerous processes have been developed for the synthesis of MnO_2 nanoparticles with different morphologies and different crystallographic forms. Nanorods and nanowires of α-, β-, γ-, and δ-MnO_2 have been prepared by several researchers.[11−18] Recently, α-MnO_2 core−shell structure with spherically aligned nanorods was prepared by Xie and co-workers.[14] Zhang et al.[17] obtained β-MnO_2 nanowires through heat treatment of MnOOH, which was synthesized from $KMnO_4$ at 180 °C for 24 h. Li and Co-workers[12] have prepared α-MnO_2 nanowires and β-MnO_2 nanorods by oxidizing $MnSO_4$ by $(NH_4)_2S_2O_8$ under low-temperature hydrothermal synthesis. Rossouw et al.[18] have synthesized α-MnO_2 nanoparticles by sulfuric acid treatment of Li_2MnO_3; Muraoka et al.[19] have reported α-MnO_2 preparation from hollandite-type (NH_4)-xMn_8O_{16}. Ye and co-workers[20] have prepared α- and γ-MnO_2 nanorods by redox reaction between $KMnO_4$ and $MnCl_2$ in the presence of polyethylene glycol and polyacrylamide polymers. Sun et al.[21] have also reported the synthesis of MnOOH and β-MnO_2 whiskers using the cationic surfactant cetyltrimethylammonium bromide.

Herein, we report, for the first time, a facile one-step solution-phase shape-controlled synthetic approach. Based on this reproducible effort, transition from spherical to single crystalline β-MnO_2 nanorods with high aspect ratio has been observed through the aerial oxidation of $MnCl_2$ in variable micellar templates under alkaline condition at room temperature. Magnetic anomalies, such as low-temperature hysteresis below a blocking temperature and divergence between FC and ZFC magnetization data, of β-MnO_2 nanorods and nanospheres and their catalytic activity have been studied and demonstrated. Cyclic voltammograms and Raman spectroscopic information further substantiate the fact.

2. Experimental Section

2.1. Reagents and Instruments. All chemicals were of analytical grade and were used as received without further purification. Double distilled water was used throughout the experiment. $MnCl_2 \cdot 4H_2O$, NaOH, and acetonitrile were pur-

* Corresponding author. E-mail: tpal@chem.iitkgp.ernet.in.

10.1021/jp074803l CCC: $37.00
Published on Web 10/05/2007

chased from Sisco Rearch Laboratory (SRL), India. Sodium dodecyl benzene sulfonate (SDBS) was received from Aldrich.

TEM analysis was performed with an instrument H-9000 NAR, Hitachi, using an accelerating voltage of 300 kV. EDX spectrum was obtained by Oxford, Link, ISIS 300 instrument. XRD was done in a PW1710 diffractometer, a Philips, Holland, instrument. The XRD data were analyzed using JCPDS software. XPS and FTIR studies were performed with an ESCALAB-MK-II, UK, and a Thermo-Nicolet continuum FTIR microscope, respectively. Raman spectrum of MnO_2 nanoparticles was obtained with a Renishaw Raman microscope, equipped with a He−Ne laser excitation source emitting at a wavelength of 633 nm, and a Peltier cooled (−70 °C) charge coupled device (CCD) camera. A Leica microscope was attached and was fitted with three objectives (5×, 20×, 50×). For these experiments, the 20× objective was used. Laser power at the sample was 20 mW, and the data acquisition time was usually 30 s. The holographic grating (1800 grooves/mm) and the slit enabled the spectral resolution of 1 cm^{-1}.

2.2. Synthesis of Spherical and Rod-Shaped MnO_2 Nanoparticles. An aqueous solution containing manganese(II) chloride ($MnCl_2 \cdot 4H_2O$, 5×10^{-3} M) and sodium dodecyl benzene sulfonate (SDBS, 5×10^{-3} to 5×10^{-2} M) was stirred on a magnetic stirrer at room temperature. Under this stirring condition, aqueous NaOH solution was introduced to this reaction mixture dropwise to obtain a final concentration of 5×10^{-3} M, and the stirring was continued for 15 min. The colorless reaction mixture turned initially to light brown and finally to dark brown, which indicates the onset of the evolution of the MnO_2 nanoparticles. The spherical as well as rod-shaped particles were collected from variable surfactant concentrations.

3. Results and Discussion

3.1. Characterization of MnO_2 Nanoparticles. Crystalline phase identification was carried out by X-ray diffraction (XRD) on a PW3040/60 X-ray diffractometer with Cu Kα radiation (λ = 1.54178 Å), the operation voltage and current maintained at 40 kV and 30 mA, respectively. The XRD pattern of the as-synthesized product is shown in Figure 1a. All of the diffraction peaks of the product can be exclusively indexed to a pure tetragonal phase of β-MnO_2 (JCPDS Card, no. 24-0735, a = 4.399 Å and c = 2.874 Å) with space group $P4_2/mnm$. No peaks for other phases were observed, indicating its high purity and crystallinity. The surface property of the as-synthesized oxide was studied by X-ray photoelectron spectroscopy (XPS). Figure 1b shows the typical XPS spectra for the as-synthesized MnO_2 particles. The binding energies for Mn $2p_{3/2}$ and Mn $2p_{1/2}$ were found to be 642.1 and 653.6 eV, respectively, indicating the presence of tetravalent Mn ions in the oxide. These values agree well with those reported for MnO_2.[22]

The EDX spectrum of the product as shown in Figure 2 again ensured the presence of Mn and oxygen in the as-prepared oxide. FTIR spectroscopy is known for its high sensitivity, especially in detecting inorganic and organic species with low content. The FTIR spectra of free SDBS and the as-synthesized oxide in SDBS are presented in Figure 3. From the FTIR spectra, the absorption peaks at 420−433 cm^{-1} were assigned to the Mn−O stretching vibration of β-MnO_2. The broad contour is observed due to the overlapping of the vibrational peaks.[23]

The general feature of the vibrational modes of manganese dioxides is their low Raman activity.[24−28] In general, Raman spectroscopy is not a primary technique like X-ray diffraction for structure elucidation. So, it is necessary to calibrate it against well-crystallized materials. To take the advantage of Raman

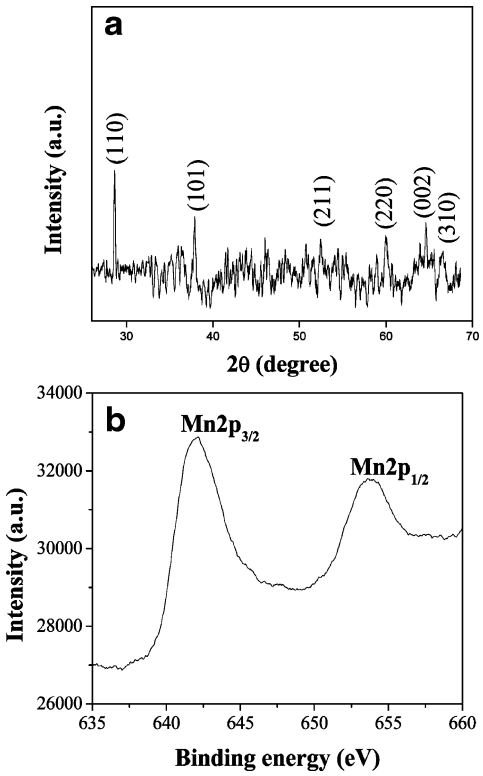

Figure 1. (a) XRD pattern and (b) XPS spectrum of β-MnO_2 nanoparticles.

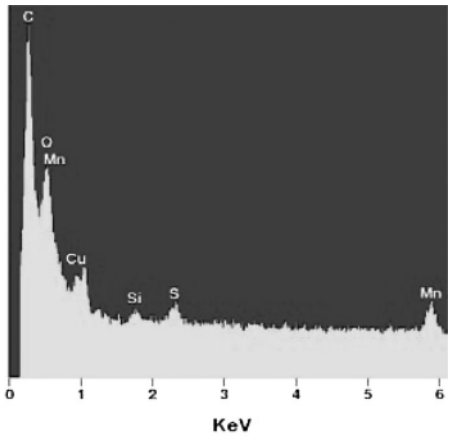

Figure 2. EDX pattern of the β-MnO_2 nanoparticles.

measurement, the instrument was calibrated against standard Si crystal to probe the short-range environment of oxygen coordination around transition metal cations in its oxide lattices.[29] Figure 4 shows the Raman scattering spectra of β-MnO_2 nanosphere and nanorods. The Raman spectrum of β-MnO_2 nanosphere is characterized by two sharp peaks at 521 and 642 cm^{-1} along with three weak bands at 288, 355, and 774 cm^{-1}, whereas for nanorods two well-defined sharp peaks appear at 521 and 644 cm^{-1} and the three weak bands at 209, 344, and 440 cm^{-1}. The two main Raman peaks correspond to the stretching mode of the MnO_6 octahedra, and the peaks at lower wavenumber are attributed to the deformation modes of the metal−oxygen chain of Mn−O−Mn in the MnO_2 octahedral lattice. Because MnO_2 is very susceptible to reduction due to laser aggression, a very low-energy He−Ne (633 nm) laser of 20 mW power was used to obtain the spectra.[30]

The morphology and the particle size of the product were determined from transmission electron microscopy. Figure 5 shows the representative TEM micrograph of MnO_2 nanopar-

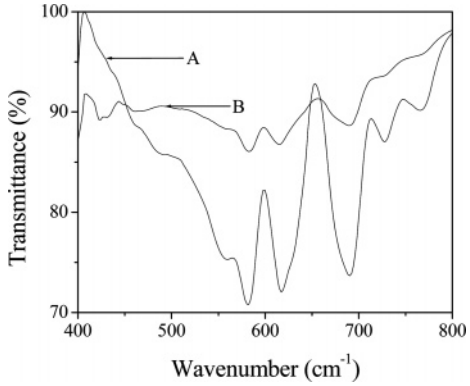

Figure 3. FTIR spectra of (A) free SDBS and (B) β-MnO_2 nanoparticles in SDBS.

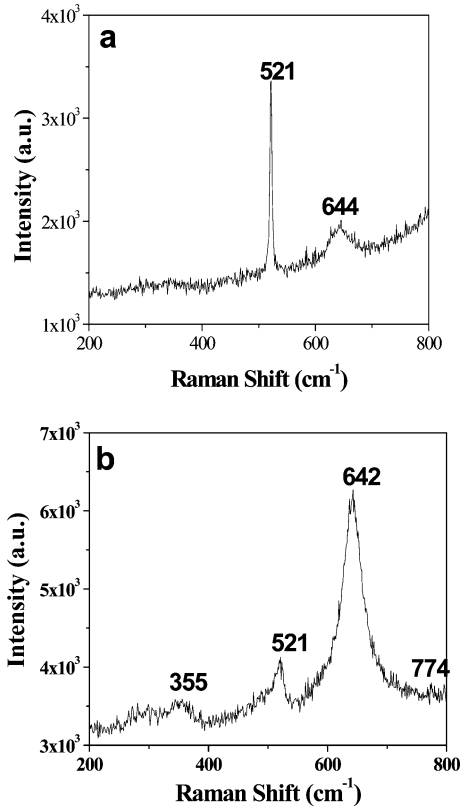

Figure 4. Raman spectra of (a) rod-shaped and (b) spherical nanoparticles of β-MnO_2.

ticles. Figure 5a shows that the sample consists of spherical nanoparticles having diameter 5 ± 2 nm, whereas Figure 5c shows the sample consists of uniform nanorods of length ~200 nm and diameter ~8 nm, that is, an aspect ratio of ~25. A variation in the concentration of SDBS (5×10^{-3} M, 10^{-2} M, and 5×10^{-2} M) successfully alters the morphology of the particles from spheres (Figure 5a) to exclusively nanorods (Figure 5c) via a mixture of spheres and rods (Figure 5b). Figure 5d represents the TEM image of a single rod, and its corresponding HRTEM (inset of Figure 5d) further demonstrates the single crystalline nature of β-MnO_2 nanorods. The fringe spacing (0.396 nm) observed in this image agrees well with the separation between (110) lattice planes.

Cyclic voltammograms of β-MnO_2 in the form of nanostructured spherical as well as rod-shaped particles show a quasi-reversible redox behavior (as shown in Figure 6), although their subtle electrochemical features widely differ depending on the morphology. For example, the rod-shaped particles formed in

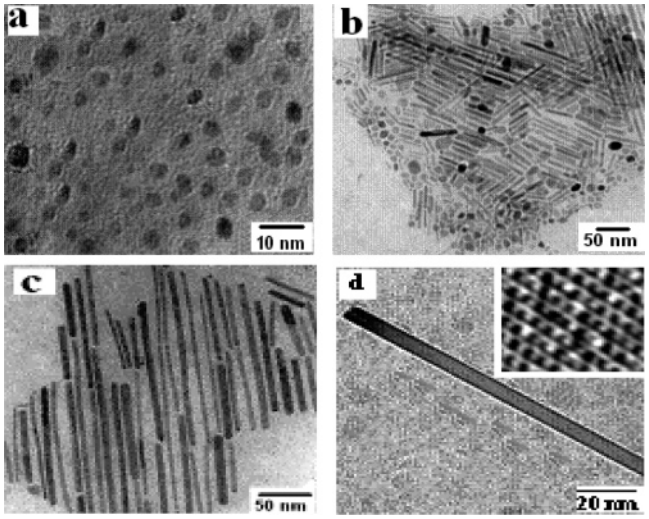

Figure 5. TEM images of β-MnO_2: (a) spherical nanoparticles, (b) mixture of spherical and rod-shaped particles, (c) nanorods, and (d) a single rod. Inset shows HRTEM image of nanorods.

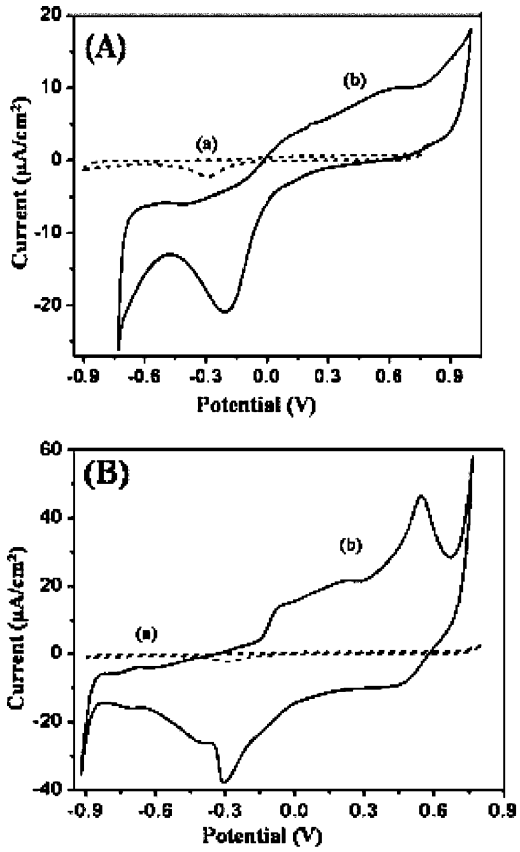

Figure 6. Cyclic voltammograms of blank Pt electrode (cycle a in both) and β-MnO_2 nanorods (b in Figure A) and nanospheres (b in Figure B) in 0.1 M NaOH at a scan rate of 100 mV/s.

the presence of SDBS (a nonredox active surfactant) give different potential (oxidation potentials at 0.125 and 0.611 V, reduction potentials at −0.201 and 0.725 V) as compared to what is known for bulk oxide on a polycrystalline Pt electrode. More interestingly, these results demonstrate the capability to distinguish the nanorods from that of corresponding nanospheres (oxidation potentials at −0.09 and 0.542 V, reduction potentials at 0.458 and −0.264 V) by virtue of their change in redox behavior.

The chemical reaction involved to synthesize β-MnO_2 nanostructures at room temperature can be formulated as follows:

$$2MnCl_2 + 4NaOH + O_2 \rightarrow 2MnO(OH)_2 + 4NaCl$$

The above reaction can be divided into the two following steps:

$$Mn^{2+} + 2OH^- \rightarrow Mn(OH)_2$$

$$2Mn(OH)_2 + O_2 \rightarrow 2MnO(OH)_2$$

Here, manganese(II) chloride at first reacts with NaOH, forms manganese hydroxide which rapidly oxidizes on exposure to air, and becomes brown due to the formation of hydrated manganese dioxide, $MnO(OH)_2$. To understand the effect of surfactant during the formation of β-MnO_2 nanorods, varying concentrations of surfactant, SDBS, were used under the same reaction conditions. It is generally assumed that micelles at concentrations close to their CMC are roughly spherical. When the surfactant concentration markedly exceeds the CMC, the shape of the spherical micelle undergoes gradual changes to assume cylindrical or lamellar structure.[31] It was observed that spherical particles of 5 ± 2 nm were produced in the presence of low concentration of SDBS (5×10^{-3} M). Upon increasing the concentration of SDBS to 10^{-2} M, the product was found to consist of a mixture of nanosphers and nanorods having an aspect ratio of ~10. While the concentration of SDBS was increased further to 5×10^{-2} M, uniform nanorods of β-MnO_2 with a diameter of ~8 nm and length of ~200 nm were observed. It should be noted that the CMC of SDBS is 1.2×10^{-3} M. Thus, the rod-like micellar template contributes to the rod formation as well as stabilizes them over the years. Furthermore, the above-mentioned experimental phenomena inspire us to speculate that it would be possible to tailor the shape of MnO_2 nanoparticles only by varying the concentration of SDBS, keeping other experimental conditions unaltered.

3.2. Magnetic Study. The magnetic properties of β-MnO_2 nanorods and nanospheres were individually characterized by SQUID magnetometer. Here, the shape-dependent change in magnetic property has been depicted for the first time. The field dependence magnetization curve (Figure 7a) of the nanorods at 77 K reveals that a superparamagnetic state exists at this temperature, as the coercive force and remnant magnetization are zero. According to the literature, when the size of the magnetic particles decreases they change from multidomain to single domain.[32] If the single domain particles become small enough, the magnetic moment in the domain fluctuates in direction due to thermal agitation, which leads to superparamagnetism. In our study, the particles, which are in the nanometer size regime, fall apparently in single domain due to which they exhibit superparamagnetism. At low temperatures, such as 2 K, the M−H curve (Figure 7b) displays a small hysteresis with coercive force of 435 Oe and remnant magnetization of 0.84 emu/g, indicating its ferromagnetic property below the blocking temperature (T_B). The T_B for nanorods has been determined to be 4 K obtained from temperature dependence magnetization studies between 0 and 60 K with zero-field-cooling (ZFC) and field-cooling (FC) in the applied field of 100 Oe, whereas for nanospheres the T_B is calculated to be 40 K as shown in Figure 8. The nanorods remain superparamagnetic until 4 K, while for nanospheres it is only 40 K. The field dependence magnetization curves for the spherical nanoparticles at 77 and 5 K are given in Figure 9. The ZFC magnetization curve shows a maximum at low temperature that is characteristic of the superparamagnetism, and the temperature at which it occurs may be taken as blocking temperature (T_B). The FC and ZFC data show divergence at low temperatures as indeed was found in the case of other oxide nanoparticles. We observed that T_B of MnO_2 nanoparticles decreases with increasing magnetic fields because less thermal energy is required to overcome superparamagnetic blocking at higher magnetic fields.

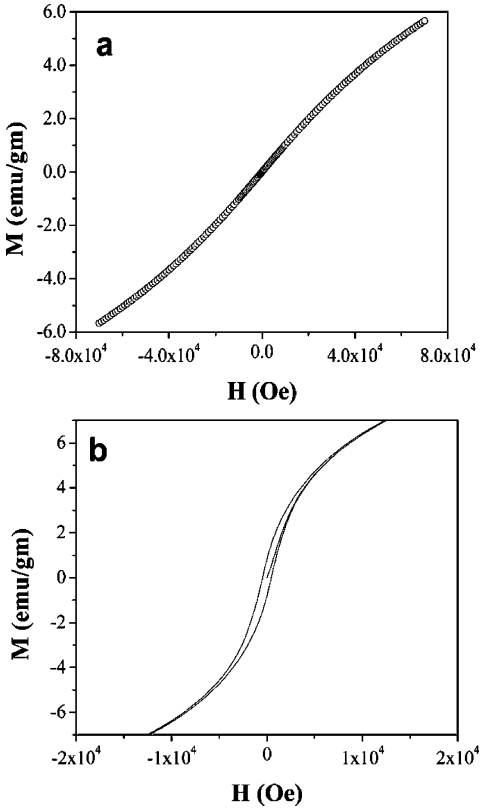

Figure 7. (a) Field dependence magnetization curves of β-MnO_2 nanorods at 77 K and (b) 2 K.

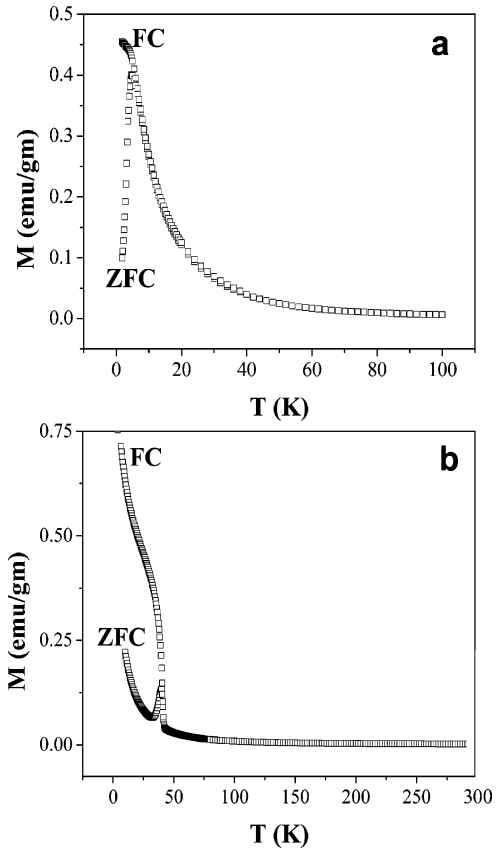

Figure 8. Magnetization versus temperature curve at an applied field of 100 Oe: (a) rod-shaped and (b) spherical β-MnO_2 nanoparticles.

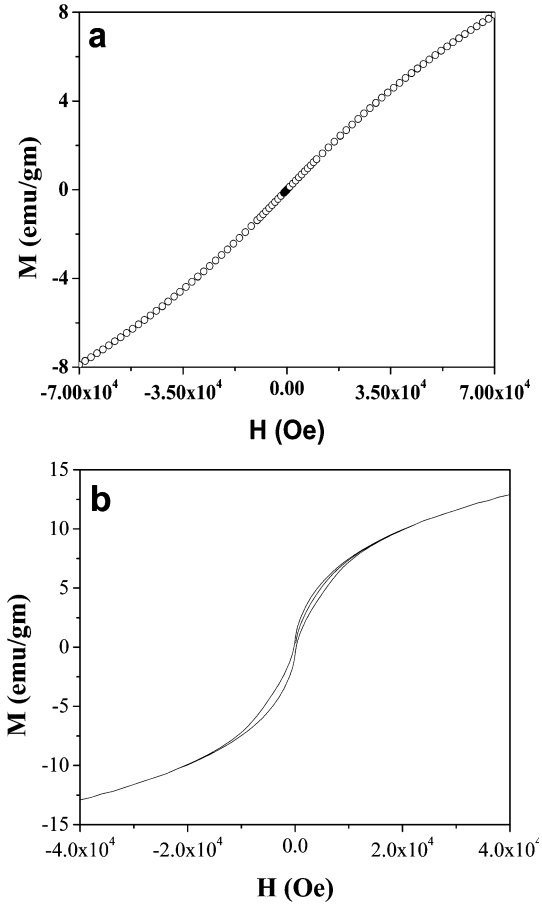

Figure 9. Field dependence magnetization curve of β-MnO_2 nanospheres at (a) 77 K and (b) 5 K.

For a superparamagnet, hysteresis is observed below blocking temperature. Above blocking temperature, the temperature overcomes the particle anisotropy energy barrier and they behave as paramagnets with very high magnetic moment: they are said to be unblocked. Therefore, at higher temperature ($T > T_B$), hysteresis disappears. However, it is already established that because of the confinement in the nanoscale, nanomaterials can exhibit unusual magnetic behaviors that are quite different from those of conventional bulk materials and their magnetic properties are highly sensitive to size and shape. As compared to spherical nanoparticles, one-dimensional nanostructures have increased anisotropies in both the shape anisotropy and the magnetocrystalline anisotropy, which exert influence on their magnetic properties.[33−35] Shape anisotropy can increase the coercivity.[21] Enhanced anisotropy induces large magnetic coercivity, where the magnetic spins are preferentially aligned along the long axis and their reversal to the opposite direction requires higher energies than that for spheres.[36] Furthermore, the shape of rods is advantageous because, using the same volume of material as a corresponding nanosphere, the nanorod will exhibit a greater dipole moment under the application of the same magnetic field.[37]

3.3. Catalytic Application. Finally, the as-synthesized MnO_2 nanoparticles (spheres and rods) have been successfully exploited as a novel catalyst for the hydrolysis of acetonitriles to acetamides in the presence of visible light under weakly basic medium. In a glass reaction vessel, 10 mL of neat acetonitrile was taken along with 0.5 mL of as-prepared β-MnO_2 nanoparticles and 200 μL of Et_3N. Next, the reaction mixture was irradiated under visible light (40 W tungsten lamp) for 10 h. After that, the product was isolated from the reaction mixture by evaporation and solvent extraction. Finally, the product was characterized via TLC, IR, and GC−MS studies. Figure 10 demonstrates the mass spectrum of acetamide. The mass spectrum showed its molecular ion peak at *m*/*z* 59. The other prominent peaks are formed at *m*/*z* 44 and 43 due to the loss of CH_3 and NH_2 groups, respectively. A comparative account for the shape-selective catalytic activity of β-MnO_2 nanoparticles revealed that rod-shaped particles are superior to spherical particles. The detail mechanistic aspect of shape selective catalysis is under investigation. It may be mentioned that commercially available MnO_2 could not produce acetamide from acetonitrile under the same reaction protocol even after 24 h.

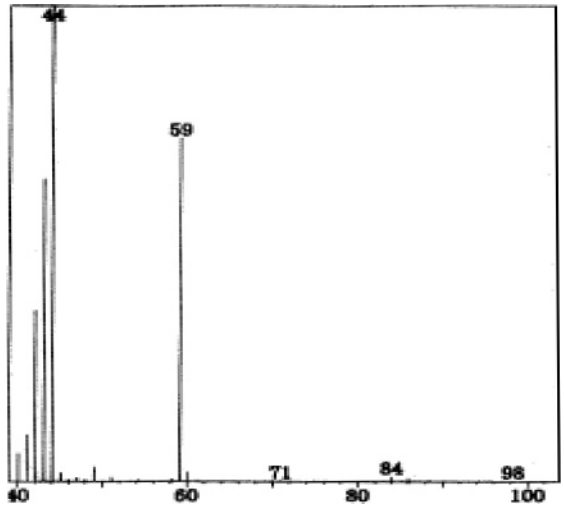

Figure 10. Mass spectrum of acetamide.

4. Conclusion

A new synthetic route is unveiled for controlled evolution of exclusively single crystalline nanospheres and nanorods with very high aspect ratio of β-MnO_2 through air oxidation of $MnCl_2$ in variable micellar template under alkaline condition at room temperature. Cyclic voltammetric studies well characterize the nanorods and nanospheres. Magnetization measurements indicate their superparamagnetic nature, and below blocking temperature they show ferromagnetic behavior, which is different from the magnetic properties of bulk β-MnO_2. Finally, the spherical and rod-shaped nanoparticles have been exploited as a novel catalyst for the hydrolysis of nitrile to amides. They may show possible novel electronic property induced by their dimensionality. Nevertheless, such a catalyst-free, cost-effective, and solution-based route for shape-selective synthesis might bring new light for large-scale production of 1D nanostructure materials.

Acknowledgment. We are thankful to the Council of Scientific and Industrial Research (CSIR), the University Grant Commission (UGC), the Department of Science and Technology (DST), New Delhi, and the Indian Institute of Technology, Kharagpur, for financial assistance. Dr. Junichi Nishijo of IMS, Japan, is gratefully acknowledged for magnetic study, and Dr. Vijayamohanan of NCL, Pune, is acknowledged for cyclic voltammetric measurements.

References and Notes

(1) Nalwa, H. S. *Handbook of Nanostructured Materials and Nanotechnology*; Academic Press: New York, 2000.

(2) Burda, C.; Chen, X. B.; Narayanan, R.; El-Sayed, M. A. *Chem. Rev.* **2005**, *105*, 1025.

(3) Duan, X.; Huang, Y.; Cui, Y.; Wang, J.; Lieber, C. M. *Nature* **2001**, *409*, 66.
(4) Xia, Y. N.; Yang, P. D.; Sun, Y. G.; Wu, Y. Y.; Mayers, B.; Gates, B. *Adv. Mater*. **2003**, *15*, 353.
(5) Sun, S.; Murray, C. B.; Weller, D. *Science* **2000**, *287*, 1989.
(6) Bruchez, M.; Moronne, M.; Gin, P. *Science* **1998**, *281*, 2013.
(7) Jana, S.; Praharaj, S.; Panigrahi, S.; Basu, S.; Pande, S.; Chang, C. H.; Pal, T. *Org. Lett.* **2007**, *9*, 2191.
(8) Thackeray, M. M. *Prog. Solid State Chem.* **1997**, *25*, 1.
(9) Liu, B.; Zeng, H. C. *J. Am. Chem. Soc.* **2004**, *126*, 8124.
(10) Wu, C.; Xie, Y.; Wang, D.; Yang, J.; Li, T. *J. Phys. Chem. B* **2003**, *107*, 13583.
(11) Wang, X.; Li, Y. *Chem. Commun.* **2002**, *7*, 764.
(12) Wang, X.; Li, Y. *J. Am. Chem. Soc*. **2002**, *124*, 2880.
(13) Perez-Binito, J. F.; Arias, C.; Amat, E. *J. Colloid Interface Sci.* **1995**, *177*, 288.
(14) Li, Z. Q.; Ding, Y.; Xiong, Y. J.; Yang, Q.; Xie, Y. *Chem. Commun*. **2005**, *7*, 918.
(15) Yuan, Z. Y.; Zhang, Z. L.; Du, G. H.; Ren, T. Z.; Su, B. L. *Chem. Phys. Lett.* **2003**, *378*, 349.
(16) Al-Sagheer, F. A.; Zaki, M. I. *Colloids Surf., A* **2000**, *173*, 193.
(17) Zhang, Y. C.; Qiao, T.; Hu, X. Y.; Zhou, W. D. *J. Cryst. Growth* **2005**, *280*, 652.
(18) Rossouw, M. H.; Liles, D. C.; Thackeray, M. M. *Mater. Res. Bull.* **1992**, *27*, 221.
(19) Muraoka, Y.; Chiba, H.; Atou, T.; Kikuchi, M.; Hiraga, K.; Syono, Y.; Sugiyama, S.; Yamamoto, S.; Grenier, J. C. *J. Solid State Chem.* **1999**, *144*, 136.
(20) Ye, C.; Lin, Z. M.; Yan, J. X. *Solid State Commun.* **2005**, *133*, 121.
(21) Folch, B.; Larionova, J.; Guari, Y.; Guerin, C.; Reibel, C. *J. Solid State Chem.* **2005**, *178*, 2368.
(22) Wang, G.; Tang, B.; Zhuo, L.; Ge, J.; Xue, M. *Eur. J. Inorg. Chem*. **2006**, 2313.
(23) Xiong, Y.; Xie, Y.; Li, Z.; Wu, C. *Chem.-Eur. J*. **2003**, *9*, 1645.
(24) Strohmeier, B. R.; Hercules, D. M. *J. Phys. Chem.* **1984**, *88*, 4923.
(25) Kapteijn. F.; van Langeveld, A. D.; Moulijn, J. A.; Andreini, A.; Vuurman, M. A.; Turek, A. M.; Jehng, J. M.; Washs, I. E. *J. Catal.* **1994**, *150*, 94.
(26) Gosztola, D.; Weaver, M. J. *J. Electranal. Chem. Interfacial Electrochem.* **1989**, *271*, 141.
(27) Bernard, M. C.; Hugot-Le, G. A.; Thi, B. V.; Cordoba de Torresi, S. *J. Electrochem. Soc*. **1993**, *140*, 3065.
(28) Buciuman, F.; Patcas, F.; Craciun, R.; Zahn, D. R. T. *Phys. Chem. Chem. Phys.* **1999**, *1*, 185.
(29) Julien, C. *Solid State Ionics* **2000**, *887*, 136−137.
(30) Julien, C.; Massot, M.; Rangan, S.; Lemal, M.; Guyomard, D. *J. Raman Spectrosc.* **2002**, *33*, 223.
(31) Fendler, J. H.; Fendler, J. E. *Catalysis in Micellar and Macromolecular System*; Academic Press: New York, 1975; p 32.
(32) Amin, N.; Arajs, S.; Matijevic, E. *Phys. Status Solidi A* **1985**, *104*, K65.
(33) Park, S. J.; Kim, S.; Lee, S.; Kim, Z. G.; Char, K.; Hyeon, J. *J. Am. Chem. Soc.* **2000**, *122*, 8581.
(34) Néél, L. In *Low-Temperature Physics*; Dewitt, C., Dreyfus, B., Degennes, P. G., Eds.; Gordon and Beach: London, 1962; p 411.
(35) Dumestre, F.; Chaudret, B.; Amines, C.; Fromen, M. C.; Casanove, M. J.; Renaud, P.; Zurcher, P. *Angew. Chem., Int. Ed.* **2002**, *41*, 4286.
(36) Seo, W. S.; Jo, H. H.; Lee, K.; Kim, B.; Oh, S. J.; Park, T. *Angew. Chem., Int. Ed.* **2004**, *43*, 1115.
(37) Dravid, V. P.; Aslam, M. *Nanoscape* **2005**, *2*, 67.